Measurement of optical losses in a high-finesse 300 m filter cavity for broadband quantum noise reduction in gravitational-wave detectors

Eleonora Capocasa,[1,2,*] Yuefan Guo,[3] Marc Eisenmann,[4] Yuhang Zhao,[1,5] Akihiro Tomura,[6] Koji Arai,[7] Yoichi Aso,[1] Manuel Marchiò,[1] Laurent Pinard,[8] Pierre Prat,[2] Kentaro Somiya,[9] Roman Schnabel,[10] Matteo Tacca,[11] Ryutaro Takahashi,[1] Daisuke Tatsumi,[1] Matteo Leonardi,[1] Matteo Barsuglia,[2] and Raffaele Flaminio[4,1]

[1]*National Astronomical Observatory of Japan, 2-21-1 Osawa, Mitaka, Tokyo 181-8588, Japan*
[2]*Laboratoire Astroparticule et Cosmologie (APC), 10 rue Alice Domon et Léonie Duquet, 75013 Paris, France*
[3]*Beijing Normal University No. 19, XinJieKouWai St., HaiDian District, Beijing 100875, People's Republic of China*
[4]*Laboratoire d'Annecy-le-Vieux de Physique des Particules (LAPP), Université Savoie Mont Blanc, CNRS/IN2P3, F-74941 Annecy-le-Vieux, France*
[5]*Department of Astronomical Science, SOKENDAI, 2-21-1 Osawa, Mitaka, Tokyo 181-8588, Japan*
[6]*The University of Electro-Communications 1-5-1 Chofugaoka, Chofu, Tokyo F-69622, Japan*
[7]*LIGO, California Institute of Technology, Pasadena, California 91125, USA*
[8]*Laboratoire des Matériaux Avancés, CNRS-IN2P3, Université de Lyon, 182-8585 Villeurbanne, France*
[9]*Graduate School of Science and Technology, Tokyo Institute of Technology, 2-12-1 Oh-okayama, Meguro, Tokyo 152-8551, Japan*
[10]*Institut für Laserphysik und Zentrum fur Optische Quantentechnologien der Universitat Hamburg, Luruper Chaussee 149, 22761 Hamburg, German*
[11]*Nikhef, Science Park, 1098 XG Amsterdam, Netherlands*

(Received 27 May 2018; published 31 July 2018)

Earth-based gravitational-wave detectors will be limited by quantum noise in a large part of their spectrum. The most promising technique to achieve a broadband reduction of such noise is the injection of a frequency-dependent squeezed vacuum state from the output port of the detector, with the squeeze angle rotated by the reflection off a Fabry-Perot filter cavity. One of the most important parameters limiting the squeezing performance is represented by the optical losses of the filter cavity. We report here the operation of a 300 m filter cavity prototype installed at the National Astronomical Observatory of Japan. The cavity is designed to obtain a rotation of the squeeze angle below 100 Hz. After achieving the resonance of the cavity with a multiwavelength technique, the round trip losses have been measured to be between 50 and 90 ppm. This result demonstrates that with realistic assumptions on the input squeeze factor and the other optical losses, a quantum noise reduction of at least 4 dB in the frequency region dominated by radiation pressure can be achieved.

DOI: 10.1103/PhysRevD.98.022010

I. INTRODUCTION

Following the ground-breaking first gravitational-wave observations [1,2], the detectors Advanced Virgo and Advanced LIGO will undergo a series of sensitivity upgrades alternating with scientific data-taking periods. In parallel the Japanese detector KAGRA is being commissioned and it will soon join the gravitational-wave detector network.

The design sensitivity of Advanced Virgo [3], Advanced LIGO [4], and KAGRA [5] is expected to be limited in a large part of the spectrum by the quantum nature of light, through its manifestations as shot noise and radiation pressure noise. As pointed out by Caves in 1981, both shot noise and radiation pressure originate from the vacuum fluctuations entering the detector from its output port [6]. The possibility to manipulate the quantum noise by injecting a broadband squeezed vacuum field [7], with a frequency-dependent squeeze angle, from the detector's output port was also proposed by Caves [6].

The production of broadband frequency-independent squeezed vacuum is a mature technology and recently 15 dB of broadband squeezed vacuum field was observed [8]. Its effectiveness was successfully tested first in a prototype [9] and then in full-scale detectors, such as GEO600 [10] and LIGO [11]. As a first step, a frequency-independent squeezed vacuum source will be injected into

*eleonora.capocasa@nao.ac.jp

Advanced Virgo and Advanced LIGO, allowing to mitigate the shot noise at the expense of an increase of the radiation pressure noise at low frequency. For the moment this does not represent an issue, since other noises limit the sensitivity in that frequency region.

To obtain a broadband noise reduction, the injected squeezed vacuum has to undergo a frequency-dependent rotation which counteracts the one induced by the opto-mechanical coupling inside the interferometer [12]. In order to achieve an optimal noise reduction, the rotation has to take place at the frequency where the radiation pressure noise crosses the shot noise, which is around 40–70 Hz for Virgo, LIGO, and KAGRA.

A technique to impress a frequency dependence on the squeeze ellipse consists in reflecting a frequency-independent squeezed vacuum field off a detuned Fabry-Perot cavity, known as a *filter cavity* [13]. Such a reflection induces a differential phase change on the upper and lower vacuum sidebands, resulting in a frequency-dependent rotation of the vacuum quadrature. The rotation frequency depends on the cavity storage time, which is proportional to the product of the finesse and the cavity length.

The possibility to achieve high levels of frequency-dependent squeezing is mainly limited by optical losses. In particular, optical losses of the filter cavity (mainly due to mirror defects) are expected to degrade the squeezing at low frequency, in the region where the squeezed vacuum field experiences the rotation. It has been shown that such an effect depends on the loss per unit length [14] and is reduced when the length of the cavity increases [15].

At present, squeezed vacuum rotation has been demonstrated in the MHz [16] and kHz regions [17]. A 300 m filter cavity prototype is being developed at the National Astronomical Observatory of Japan, using the vacuum system and the seismic isolation system originally built for the TAMA interferometer. The goal of the experiment is to demonstrate frequency-dependent squeezing, with a rotation angle below 100 Hz, in the region where the rotation is needed for Virgo, LIGO, and KAGRA. The design of the cavity was presented in a previous publication [18].

We report here the operation of the cavity with a multiwavelength control system, the measurement of the optical losses, their comparison with the expected values, and their impact on the quantum noise reduction. The integration of the squeezed vacuum source is still ongoing.

The article is organized as follows. In the next section we describe the experimental setup. In Sec. III we describe the requirements for mirror surface quality and the results of the mirror surface characterization. In Sec. IV we present the measurements of the optical losses. Finally, in Sec. V we present our conclusions and discuss planned next steps.

II. EXPERIMENTAL SETUP

The experimental setup is composed of three parts: the source of a broadband squeezed vacuum field with frequency-independent squeeze angle, the optics needed to inject the squeezed beam into the cavity, and the suspended cavity itself. The relevant parameters of the experiment are reported in Table I and an overall schematic of the setup is shown in Fig. 1.

A. Squeezed vacuum source

The design of the squeezed vacuum source (or *squeezer*) is based on the design and experience of the GEO600 squeezer [19]. The main laser—a 2 W, 1064 nm Nd:YAG laser—is used to pump the second harmonic generator (SHG) cavity, which doubles the laser frequency, producing green light at 532 nm.

In our scheme, this green light is split into two beams that are used for two different purposes. A part of the beam is used to pump the optical parametric oscillator for the squeezed vacuum production. The other part is injected into the filter cavity and used to lock the main laser frequency to the cavity length by means of a Pound-Drever-Hall detection scheme [20].

The beam used for the control of the filter cavity passes through an acousto-optic modulator (AOM), which induces a tunable frequency shift and is used to control the detuning of the infrared (squeezed) beam with respect to the cavity resonance. The infrared beam transmitted by the first beam splitter (placed before the SHG) is used in part as a local oscillator for the homodyne detection and in part as a temporary probe beam to characterize the filter cavity.

At the time of writing, the SHG has been assembled and locked. A part of the produced green beam is used to lock the filter cavity and the infrared light transmitted by the first beam splitter is superposed to the green one and made to resonate in the cavity by driving the AOM frequency.

TABLE I. Summary of the filter cavity parameters. In the first column shows the design values, while the second column shows the actual values. Mirrors transmissivity and radius of curvature are measured at LMA. The finesse has been estimated from the mirror transmissivity, assuming round trip losses of 60 ppm (as predicted by the results of the mirror characterization).

Cavity parameter	Design	Real value
Length	300 m	300 m
Mirror diameter	10 cm	10 cm
Input mirror radius of curvature	415 m	438 m
End mirror radius of curvature	415 m	445 m
Input mirror transmissivity (1064 nm)	0.14%	0.136%
End mirror transmissivity (1064 nm)	<5 ppm	3.9 ppm
Finesse (1064 nm)	4290	4425
Input mirror transmissivity (532 nm)	1.4%	0.7%
End mirror transmissivity (532 nm)	1.4%	2.9%
Finesse (532 nm)	445	172
Beam diameter at waist	1.65 cm	1.68 cm
Beam diameter at the mirrors	2.06 cm	2.01 cm

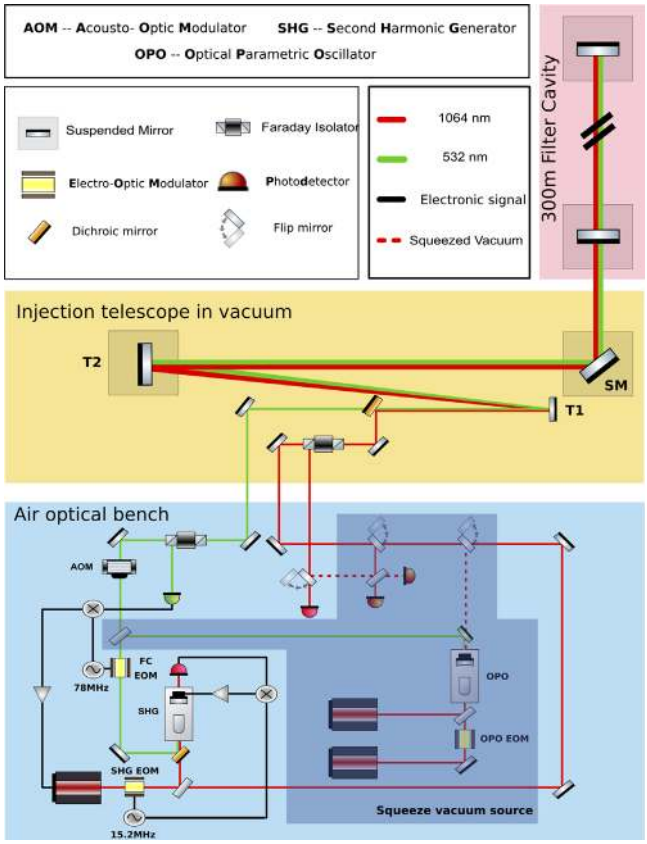

FIG. 1. Overall scheme of the experiment. The installation of the components in the grey shaded area of the optical table is currently ongoing.

The remaining components are assembled and their installation is ongoing.

B. Injection path

As shown in Fig. 1, the infrared beam and the green beam are separately injected into the vacuum system. The infrared beam passes through an in-vacuum Faraday isolator that is used to extract the infrared light reflected by the cavity. In the final setup this will be replaced by the frequency-dependent squeezed vacuum beam and will be sent to the homodyne detector. In the present setup, the reflected infrared beam is sensed by a photodiode, in order to perform the loss measurements described in this article and to monitor its detuning from the cavity resonance. After passing through the Faraday isolator, the infrared beam is superposed to the green beam by means of a dichroic mirror. The superposed beams are then magnified by a factor of 10 using an afocal reflective telescope. This consists of two spherical mirrors (T1 and T2 in Fig. 1) with radii of curvature (RoC) of −0.6 m (convex) and 6 m (concave), respectively, at a distance of 2.7 m. After the telescope, the beams are reflected toward the filter cavity by a flat steering mirror with a diameter of 15 cm (SM in Fig. 1). The mirror T2 of the telescope and the steering mirror are both suspended. By adjusting their alignment, it is possible to align the beams on the cavity axis.

C. Filter cavity suspensions and alignment

Four suspended mirrors are used in our setup: two are part of the injection system described above, and two are the mirrors composing the filter cavity. The suspension system consists of a double pendulum originally developed for the TAMA experiment [21]. It is composed of a top stage to which four wires are attached and used to suspend an intermediate mass. A passive damping system consisting of a set of magnets placed around this intermediate mass is installed. The mirror, with a diameter of 10 cm, is suspended with two loop wires from the intermediate mass. Four magnets are glued to the backs of the mirrors, allowing to move them by coil actuators. The double pendulum is placed on a vibration isolation multilayer stack made of rubber and metal blocks [22].

The mirror position is sensed using optical levers with lenses which decouple shifts and tilt motion [23]. The output of such systems is used as the error signal for a local control loop which keeps the mirror motion in the range of a few μrad and allows us to align the cavity. After centering the green beam on the end mirror by using the suspended steering mirrors, the cavity is aligned by adjusting the position of the input and end mirrors to maximize the transmitted green power. At that point the infrared beam is aligned by using two steering mirrors on the optical table, in order to coalign it to the cavity axis and maximize its transmitted power.

D. Filter cavity control

The filter cavity is kept resonant with the green beam using a standard Pound-Drever-Hall scheme in reflection and acting on the main laser frequency. The correction signal to the laser piezo is provided by an analog servo, with a bandwidth of about 20 kHz. In order to also make the infrared beam resonant in the cavity, the relative frequency of the green and infrared beams is adjusted by driving the AOM placed on the green path. The frequency shift necessary to achieve simultaneous resonance has been observed to be stable on the time scale of the green lock duration, that is, a few hours. In order to achieve the rotation of the squeeze ellipse, this value will be adjusted to operate the cavity at the proper detuning [18,24]. The cavity characterization has been performed using a bright IR beam which will be replaced with squeezed vacuum in the future. The lock accuracy, measured as the rms of the Pound-Drever-Hall error signal, is ∼120 Hz for the green beam, while that of the IR is of the order of a few Hz. The difference between the two lock accuracies is explained by the fact that, due to the higher finesse of the cavity for the IR beam, the laser noise is more filtered at high frequency, above the pole of the cavity, where most of the rms accumulates.

III. CAVITY MIRROR REQUIREMENTS AND CHARACTERIZATION

The degradation of the squeeze factor induced by several loss sources has been modeled, taking into account losses in the injection and readout paths, the effect of mismatching (between the squeezer and the cavity, and between the squeezer and the local oscillator), phase noise, and filter cavity losses [24]. Filter cavity losses have been shown to be one of the main contributors to squeezing degradation at low frequency, in the region over which the squeezing ellipse rotation takes place, limiting the quantum noise reduction in the radiation-pressure-dominated region. Since they are mainly caused by scattering from mirror defects, the requirements on the mirror quality have been carefully set after performing a complete squeezing degradation budget [18]. We set the round-trip loss requirement to 80 ppm. This level, combined with other sources of squeezing degradation (whose expected levels are reported in Table II) should allow for a squeezing level of about 4 dB at low frequency and 6 dB at high frequency [18]. The threshold of 80 ppm has been chosen because the associated squeezing degradation at low frequency is comparable with the one expected from the optimistic level of mode mismatching expected for advanced gravitational-wave detectors (reported in Table II), and therefore lower losses would not increase the squeezing level unless the mismatching is also reduced.

The value of 80 ppm includes the losses induced by low-spatial-frequency defects, up to 10^3 m^{-1} (contributing to the so-called mirror *flatness*), the losses due to higher-frequency defects (contributing to the so-called mirror *roughness*), and the ones due to point defects. The first ones are estimated by performing simulations with maps usually obtained from wave-front measurements with a phase-shifting interferometer [25], while the latter can be directly measured by recording the scattered light at angles larger than a few degrees.

By performing fast Fourier transform (FFT) simulations with real mirror maps, using the MATLAB-based optical FFT code OSCAR [26], we set the specification on the mirror peak valley (PV) to be less than 12.7 nm on a diameter of 0.05 m and less than 6.3 nm on a diameter of 0.02 m.

TABLE II. Parameters used in the estimation of squeezing degradation done in Ref. [18] allowing to reach 4 dB of squeezing at low frequency.

Squeezing degradation parameter	Value
Filter cavity losses	80 ppm
Injection losses	5%
Readout losses	5%
Mode-mismatch squeezer-filter cavity	2%
Mode-mismatch squeezer-local oscillator	5%
Filter cavity length noise (RMS)	0.3 pm
Injected squeezing	9 dB

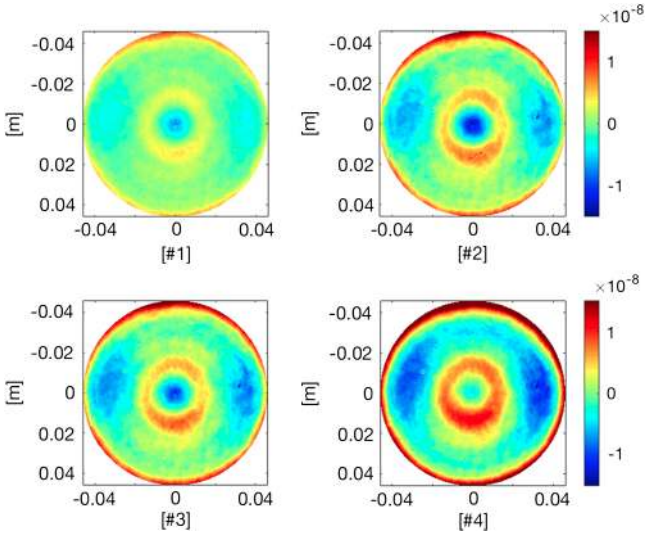

FIG. 2. Measured flatness maps of the four filter cavity mirrors. Mirrors #1 and #4 have been installed.

Four mirrors have been purchased for the filter cavity and they have been coated and characterized at the Laboratoire des Matériaux Avancés (LMA) in Lyon. The measured maps are plotted in Fig. 2. The results of this characterization are reported in Table III and show that the mirror flatness is compliant with our requirements.

The pair of mirrors to be installed is chosen by performing FFT simulations of the cavity using the measured mirror maps. The round trip losses for the four combinations are plotted in Fig. 3 as a function of the deviation from the nominal radius of curvature. They all show a round-trip loss floor of ∼40 ppm, which agrees with our requirement. They also show peaks in the losses due to power transferred to higher-order modes that are partially resonant for some values of the two curvature radii. We chose the pair for which the peaks in the losses due to higher-order mode resonances are more distant from the nominal RoC value. It corresponds to input mirror number 4 and end mirror number 1 (red line in Fig. 3).

In order to have a complete estimation of the round-trip losses, we should add up all of the contributions: those from the flatness given from the simulation (∼40 ppm), those

TABLE III. RMS and PV (over different diameters) for the four mirror substrates measured at LMA.

	Diameter 0.05 m		Diameter 0.02 m	
Mirror	RMS (nm)	PV (nm)	RMS (nm)	PV (nm)
#1	2.0	11.5	0.52	3.3
#2	2.1	12.2	0.52	3.3
#3	1.5	8.3	0.48	3.4
#4	1.9	14.8	0.48	3.4

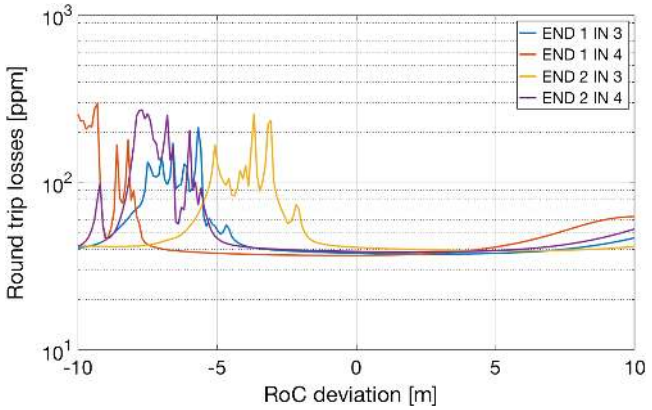

FIG. 3. Round trip losses for different combinations of filter cavity mirrors as a function of the deviation from the measured RoCs. The peaks are due to higher-order modes partially resonant for some values of the two curvature radii. The combination of mirrors #1 and #4 is thus optimal from this point of view.

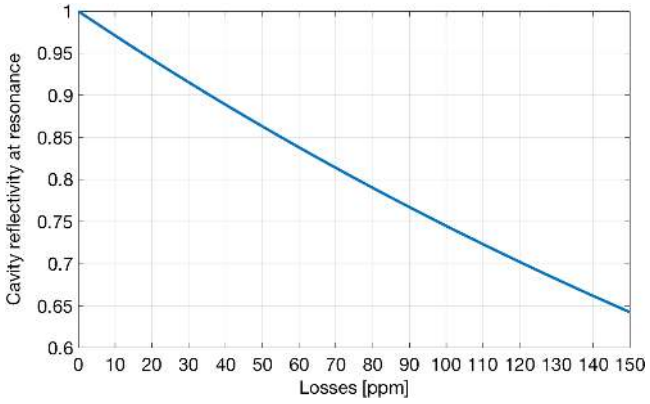

FIG. 4. Change of the cavity reflectivity as a function of the round-trip losses.

from roughness and point defects (measured to be ∼9 ppm and ∼5 ppm for the input and the end mirror respectively), and those from absorption and transmission from the end mirror (∼5 ppm). Therefore, the total round trip losses are expected to be ∼60 ppm.

IV. ROUND-TRIP LOSS MEASUREMENTS

The round-trip losses in a Fabry-Perot cavity are defined via energy conservation as [27]

$$L = \frac{P_{\mathrm{in}} - P_{\mathrm{r}} - P_{\mathrm{t}}}{P_{\mathrm{circ}}}, \tag{1}$$

where P_{in} is the input power, and P_{circ}, P_{t}, and P_{r} are the power circulating in the cavity and the transmitted and reflected powers, respectively. They affect different optical parameters such as the finesse, the decay time, and the cavity power reflectivity which are defined, respectively, as [28]

$$F = \frac{\pi\sqrt{r_1 r_2}}{1 - r_1 r_2}, \tag{2}$$

$$\tau = -\frac{1}{\nu_{\mathrm{FSR}} \log(r_1 r_2)}, \tag{3}$$

$$R = \left[\frac{r_1 - r_2}{1 - r_1 r_2}\right]^2, \tag{4}$$

where r_1 and r_2 are the amplitude reflectivities of the input and end mirrors, and ν_{FSR} is the free spectral range of the cavity defined as $c/2l$ (where c is the speed of light and l is the length of the cavity).

In principle, the losses can be extrapolated from any of these quantities, e.g., by incorporating them into the end-mirror transmissivity (which in our case is below 4 ppm),

$$r_2 = \sqrt{1 - T_2} \to \sqrt{1 - L}, \tag{5}$$

where L also contains the losses due to the transmissivity of the end mirror. In practice, the extraction of the losses using the finesse and the decay time is limited by the effect of the uncertainty on the input-mirror transmissivity. In fact, a relative uncertainty of 1% on the input-mirror transmissivity (corresponding to $\Delta T \sim 0.0014\%$) results in an error of ±15 ppm of losses. Luckily, in a strongly overcoupled cavity, as in our case, the cavity reflection is a suitable quantity to measure the round-trip losses independently, as it has only a small dependence on the input-mirror transmissivity.

The reflectivity of a the cavity at resonance, with the approximation of Eq. (5), reads

$$R_{\mathrm{cav}} = \frac{P_{\mathrm{res}}}{P_{\mathrm{in}}} = \left[\frac{r_1 - r_2}{1 - r_1 r_2}\right]^2 \simeq \left[\frac{r_1 - \sqrt{1 - L}}{1 - r_1\sqrt{1 - L}}\right]^2, \tag{6}$$

where P_{res} is the reflected power on resonance and P_{in} is the incident power, which is estimated by measuring the reflected power while the cavity is set to be out of resonance.

The expected change in the cavity reflectivity induced by losses in our filter cavity is plotted in Fig. 4. We see that, e.g., a change of 3% in the reflectivity corresponds to 10 ppm of losses.

Equation (6) can be inverted and approximated [23] to find

$$L \sim \frac{T_1}{2}\frac{1 - R_{\mathrm{cav}}}{1 + R_{\mathrm{cav}}} = \frac{T_1}{2}\frac{1 - P_{\mathrm{res}}/P_{\mathrm{in}}}{1 + P_{\mathrm{res}}/P_{\mathrm{in}}}. \tag{7}$$

The losses are measured by repeatedly setting the IR beam on and off resonance, recording the consequent change in the reflected power (as shown in Fig. 6), and computing the reflectivity as the ratio between the reflected power in the two states.

A. Influence of an imperfectly coupled input beam

If a part of the incoming power does not couple with the cavity (e.g., in the presence of mismatching, misalignment, modulation sidebands, and residual frequency fluctuations due to the finite gain of the locking servo), it will be promptly reflected and will not experience losses. As a consequence, the apparent reflectivity of the cavity on resonance will increase and the measured losses will be reduced.

Assuming that the round trip losses associated with a cavity are those experienced by an input beam perfectly coupled into the cavity, we are interested in compensating the effect of uncoupled power in our reflectivity measurement. Suppose that a fraction γ of the incoming power does not couple with the cavity; the reflected power on resonance can be rewritten as

$$P^{\gamma}_{\mathrm{res}} = R_{\mathrm{cav}} P_{\mathrm{in}}(1-\gamma) + \gamma P_{\mathrm{in}}, \tag{8}$$

from which we can find an expression for $R^{\gamma}_{\mathrm{cav}}$, the cavity reflectivity in the presence of some uncoupled power,

$$R^{\gamma}_{\mathrm{cav}} = \frac{P^{\gamma}_{\mathrm{res}}}{P_{\mathrm{in}}} = R_{\mathrm{cav}}(1-\gamma) + \gamma. \tag{9}$$

Inverting the equation above, we find the relation to be used to deduce the "real" cavity reflectivity, i.e., the one found with a perfectly coupled input beam, knowing the level of uncoupled power γ and the measured reflectivity $R^{\gamma}_{\mathrm{cav}}$,

$$R_{\mathrm{cav}} = \frac{R^{\gamma}_{\mathrm{cav}} - \gamma}{(1-\gamma)}. \tag{10}$$

The change of the measured cavity reflectivity as a function of the percentage of input power not coupled into the cavity is shown in Fig. 5. The amount of mismatching and misalignment is estimated to be ∼4% by measuring the optical spectrum of the cavity and comparing the height of the higher order modes with that of the fundamental one. The power on the radio-frequency sidebands used to generate the Pound-Drever-Hall signal is ∼8% and the power lost for the residual fluctuations of the laser frequency is ∼1%. All of these contributions give ∼13% of uncoupled power in the cavity, whose effect has been compensated in the reflectivity computation with the technique explained above.

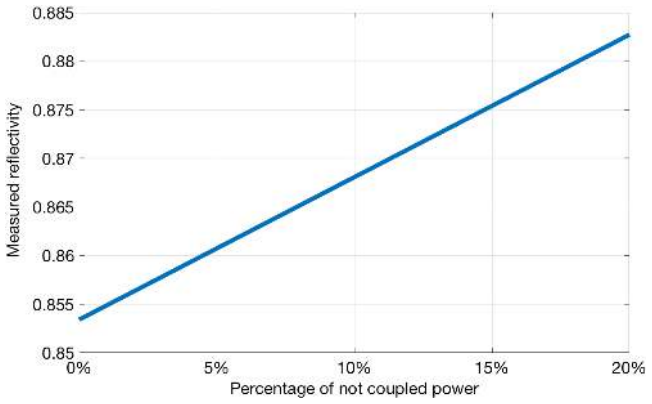

FIG. 5. Change of the measured cavity reflectivity as a function of the fraction of input power not coupled into the cavity, assuming 60 ppm of round-trip losses.

B. Data analysis and results

The on/off resonance measurements are performed several times keeping the cavity locked with the green beam and applying a frequency shift with the AOM large enough to bring the IR beam out of resonance. Figure 6 shows an example of the change in the reflected power when performing such a measurement. For each on/off resonance switch, the cavity reflectivity and, in turn, the losses are estimated from the measured ratio between the reflected powers in the resonant and nonresonant states.

The reflected power when the beam is not resonant has Gaussian fluctuations (as shown in Fig. 7), which are mainly due to the input power fluctuations, and its level can be estimated by taking the mean of the time series, with two standard deviations as the uncertainty. On the other hand, the reflected power when the cavity is resonant is subjected to additional fluctuations due to fast alignment fluctuations, finite locking accuracy, and possibly other unknown sources.

Concerning the alignment fluctuations, if the cavity is not optimally aligned, the alignment fluctuations can either increase or decrease the reflected power. On the contrary, since we assume to be locked at the top of the resonance, the fluctuations of the locking point of the cavity (due to the finite lock accuracy) can only increase the reflected power, and therefore are not expected to give a symmetric distribution of the cavity reflectivity.

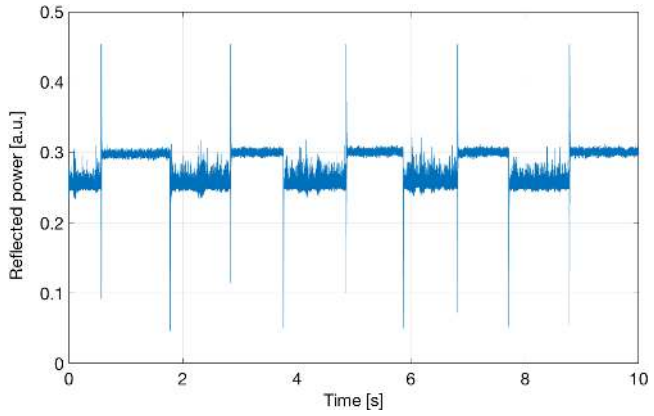

FIG. 6. Reflected power change during a set of on/off resonance switches of the IR beam. From the difference between the two levels we can estimate the cavity reflectivity and therefore the round-trip losses.

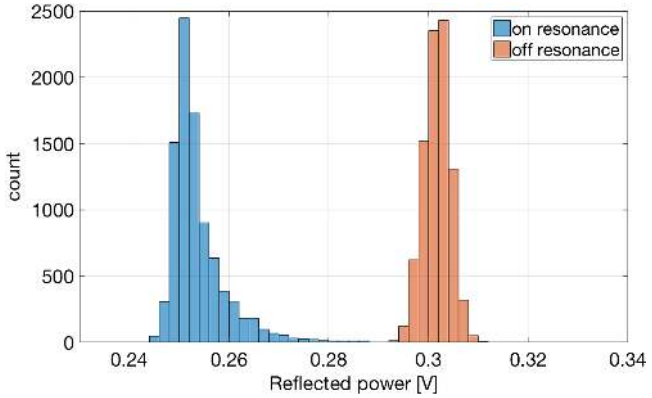

FIG. 7. A typical histogram of the reflected power time series for both a resonant and nonresonant periods. The fluctuations when the beam is not resonant are Gaussian while those when it is resonant show a broader asymmetric distribution.

We observe that the fluctuations of the reflected light when the beam is resonant usually have an asymmetric distribution. As shown in Fig. 7, the left tail with respect to the maximum value (the so-called *mode*) is Gaussian, with a standard deviation similar to that of the nonresonant state. The right tail (higher powers) is much broader.

Since the fluctuations toward the higher power (like those of the lock accuracy) give rise to an underestimation of the round-trip losses, we decide to keep a conservative approach. The highest value of the histogram is used as a representative value of the reflected power. The uncertainty of the measurement is chosen as two standard deviations of the Gaussian distribution computed using only the left tail (assuming that the left tail is given by power and alignment Gaussian fluctuations). It is important to point out that using the mode instead of the mean gives a difference of only ∼5 ppm in the estimated losses, meaning that our analysis is not strongly dependent on this choice.

For each measurement (i.e., a set of consecutive on/off resonance switches, like the one in Fig. 6) we compute the reflectivity as the mean (weighted with uncertainties) of the reflectivities obtained from each on/off resonance switch with the method described above. The results are plotted together in Fig. 8.

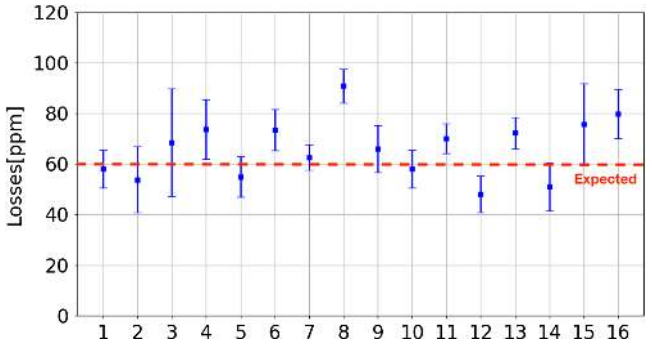

FIG. 8. Summary of the round-trip loss measurements. The scattering of the results may depend on different alignment conditions of the cavity from one day to another. The measurements have been taken on different days over about two months.

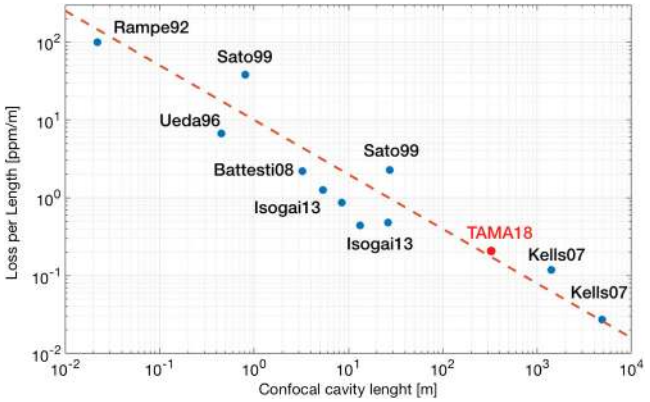

FIG. 9. The plot shows some measured round-trip losses per unit length from the literature. They were originally published in Ref. [15], then updated with measurements by Isogai *et al.* in Ref. [28]. We added the measured losses for the filter cavity in TAMA (this work). To remove any dependence on the choice of cavity geometry, the plots are shown as a function of the confocal length, i.e., the length of the confocal cavity which has the same beam dimension on the mirror as the cavity whose losses are reported. References for the measurements in the literature can be found in Ref. [15].

The measured losses are between 50 and 90 ppm (with typical error bars between ±5 and ±10 ppm), while from simulation we expect ∼60 ppm. The fluctuation of the reflectivity from one measurement to another is larger than the experimental uncertainty of each of them. This phenomenon was already observed in Ref. [28] and it is possibly due to different alignment conditions: the beam impinges on different areas of the mirrors which can have slightly different surface qualities, causing a variation in the amount of scattered light. The mean of these measurements gives ∼67 ppm of losses (0.22 ppm/m). We plot this value together with other measured round-trip losses per unit length from the literature in Fig. 9. It shows a good agreement with the empirical scaling law (dotted line in Fig. 9) extrapolated from the previous measurements [28].

V. CONCLUSIONS AND NEXT STEPS

We have shown the operation of a 300 m filter cavity designed to impress a quadrature rotation at about 70 Hz of the vacuum squeezed state, that is to be injected in future upgrades of LIGO, Virgo, and KAGRA. The cavity is controlled by using a green beam, obtained by doubling the frequency of the infrared laser used for the squeezing generation. We have been able to control the resonance condition of an infrared probe beam with an AOM. In this configuration, we could estimate the round trip losses of the cavity, which are the most critical parameter affecting the squeeze factor in the radiation-pressure-dominated region.

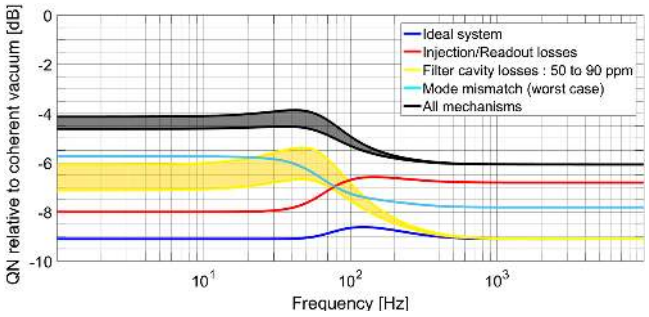

FIG. 10. Quantum noise relative to coherent vacuum (0 dB), computed taking into account different squeezing degradation mechanisms. The yellow area corresponds to the contribution from filter cavity losses between 50 and 90 ppm. The parameters used to estimate the other degradation mechanisms are those reported in Table II.

From the measurement of the cavity reflectivity using the on/off resonance technique, we obtained round-trip losses between 50 and 90 ppm, where the scattering of the results may depend on different alignment conditions of the cavity. The squeeze factor achievable with this loss level is plotted in Fig. 10, where the parameters used to estimate the other degradation mechanisms are those reported in Table II. Even with the worst results, the losses are compatible with 4 dB of squeezing in the radiation-pressure-dominated region and 6 dB of squeezing at high frequency.

The installation of the frequency-independent squeezing source is ongoing as well as the integration of an automatic alignment system, which we expect to improve the stability of the cavity and the precision and reproducibility of the loss measurements.

ACKNOWLEDGMENTS

We thank Jérôme Degallaix for fruitful discussions about the loss measurement and the help with OSCAR simulations. We thank also the Advanced Technology Center of the National Astronomical Observatory of Japan for the support. This work was supported by the JSPS Grant-in-Aid for Scientific Research (Grant No. 15H02095), the JSPS Core-to-Core Program, A. Advanced Research Networks, and the European Commission under the Framework Program 7 (FP7) "People" project ELiTES (Grant Agreement No. 295153) and EU Horizon 2020 Research and Innovation Programme under the Marie Sklodowska-Curie Grant Agreement No. 734303. E. C. was supported by the European Gravitational Observatory, by the scholarship "For Women in Science" from the Fondation l'Oréal UNESCO, and by the scholarship "Walter Zellidja" from the Académie Française.

[1] B. P. Abbott *et al.* (LIGO Scientific and Virgo Collaborations), Observation of Gravitational Waves from a Binary Black Hole Merger, Phys. Rev. Lett. **116**, 061102 (2016).
[2] B. P. Abbott *et al.* (LIGO Scientific and Virgo Collaborations), GW170817: Observation of Gravitational Waves from a Binary Neutron Star Inspiral, Phys. Rev. Lett. **119**, 161101 (2017).
[3] F. Acernese *et al.* (Virgo Collaboration), Advanced Virgo: A second-generation interferometric gravitational wave detector, Classical Quantum Gravity **32**, 024001 (2015).
[4] J. Aasi *et al.* (LIGO Scientific Collaboration), Advanced LIGO, Classical Quantum Gravity **32**, 115012 (2015).
[5] Y. Aso, Y. Michimura, K. Somiya, M. Ando, O. Miyakawa, T. Sekiguchi, D. Tatsumi, and H. Yamamoto (KAGRA Collaboration), Interferometer design of the KAGRA gravitational wave detector, Phys. Rev. D **88**, 043007 (2013).
[6] C. M. Caves, Quantum-mechanical noise in an interferometer, Phys. Rev. D **23**, 1693 (1981).
[7] R. Schnabel, Squeezed states of light and their applications in laser interferometers, Phys. Rep. **684**, 1 (2017).
[8] H. Vahlbruch, M. Mehmet, K. Danzmann, and R. Schnabel, Detection of 15 dB Squeezed States of Light and their Application for the Absolute Calibration of Photoelectric Quantum Efficiency, Phys. Rev. Lett. **117**, 110801 (2016).
[9] K. Goda, O. Miyakawa, E. E. Mikhailov, S. Saraf, R. Adhikari, K. McKenzie, R. Ward, S. Vass, A. J. Weinstein, and N. Mavalvala, A quantum-enhanced prototype gravitational-wave detector, Nat. Phys. **4**, 472 (2008).
[10] LIGO Scientific Collaboration, A gravitational wave observatory operating beyond the quantum shot-noise limit, Nat. Phys. **7**, 962 (2011).
[11] J. Aasi *et al.* (LIGO Scientific Collaboration), Enhanced sensitivity of the LIGO gravitational wave detector by using squeezed states of light, Nat. Photonics **7**, 613 (2013).
[12] M. T. Jaekel and S. Reynaud, Quantum limits in interferometric measurements, Europhys. Lett. **13**, 301 (1990).
[13] H. J. Kimble, Y. Levin, A. B. Matsko, K. S. Thorne, and S. P. Vyatchanin, Conversion of conventional gravitational-wave interferometers into quantum nondemolition interferometers by modifying their input and/or output optics, Phys. Rev. D **65**, 022002 (2001).
[14] F. Ya. Khalili, Optimal configurations of filter cavity in future gravitational-wave detectors, Phys. Rev. D **81**, 122002 (2010).
[15] M. Evans, L. Barsotti, P. Kwee, J. Harms, and H. Miao, Realistic filter cavities for advanced gravitational wave detectors, Phys. Rev. D **88**, 022002 (2013).
[16] S. Chelkowski, H. Vahlbruch, B. Hage, A. Franzen, N. Lastzka, K. Danzmann, and R. Schnabel, Experimental characterization of frequency-dependent squeezed light, Phys. Rev. A **71**, 013806 (2005).

[17] E. Oelker, T. Isogai, J. Miller, M. Tse, L. Barsotti, N. Mavalvala, and M. Evans, Audio-Band Frequency-Dependent Squeezing for Gravitational-Wave Detectors, Phys. Rev. Lett. **116**, 041102 (2016).

[18] E. Capocasa, M. Barsuglia, J. Degallaix, L. Pinard, N. Straniero, R. Schnabel, K. Somiya, Y. Aso, D. Tatsumi, and R. Flaminio, Estimation of losses in a 300 m filter cavity and quantum noise reduction in the KAGRA gravitational-wave detector, Phys. Rev. D **93**, 082004 (2016).

[19] S. Chelkowski, H. Vahlbruch, K. Danzmann, and R. Schnabel, Coherent control of broadband vacuum squeezing, Phys. Rev. A **75**, 043814 (2007).

[20] E. D. Black, An introduction to Pound–Drever–Hall laser frequency stabilization, Am. J. Phys. **69**, 79 (2001).

[21] R. Takahashi, K. Arai *et al.*, Operational status of TAMA300 with the seismic attenuation system (SAS), Classical Quantum Gravity **25**, 114036 (2008).

[22] R. Takahashi, F. Kuwahara, E. Majorana, M. A. Barton, T. Uchiyama, K. Kuroda, A. Araya, K. Arai, A. Takamori, M. Ando, K. Tsubono, M. Fukushima, and Y. Saito, Vacuum-compatible vibration isolation stack for an interferometric gravitational wave detector TAMA300, Rev. Sci. Instrum. **73**, 2428 (2002).

[23] E. Capocasa, Optical and noise studies for Advanced Virgo and filter cavities for quantum noise reduction in gravitational-wave interferometric detectors, Ph.D. thesis, Université Paris Diderot, 2017, https://tds.virgo-gw.eu/index.php?content=3&r=14356.

[24] P. Kwee, J. Miller, T. Isogai, L. Barsotti, and M. Evans, Decoherence and degradation of squeezed states in quantum filter cavities, Phys. Rev. D **90**, 062006 (2014).

[25] N. Straniero, J. Degallaix, R. Flaminio, L. Pinard, and G. Cagnoli, Realistic loss estimation due to the mirror surfaces in a 10 meters-long high finesse Fabry-Perot filter-cavity, Opt. Express **23**, 21455 (2015).

[26] J. Degallaix, OSCAR a MATLAB based optical FFT code, J. Phys. Conf. Ser. **228**, 012021 (2010).

[27] J. Degallaix, M. Galimberti, R. Bonnand, and Q. Benoit, Defining the arm cavity loss for Advanced Virgo, Scientific & Technical note, Virgo Scientific & Technical note Report No. VIR-0706A-10, https://tds.virgo-gw.eu/ql/?c=8044.

[28] T. Isogai, J. Miller, P. Kwee, L. Barsotti, and M. Evans, Loss in long-storage-time optical cavities, Opt. Express **21**, 30114 (2013).